ELSEVIER

Geomorphology 29 (1999) 93–105

GEOMORPHOLOGY

Monitoring changing position of coastlines using Thematic Mapper imagery, an example from the Nile Delta

Kevin White [a,*], Hesham M. El Asmar [b,1]

[a] *Department of Geography, The University of Reading, Whiteknights, Reading RG6 6 AB, UK*
[b] *Department of Geology, Damietta Faculty of Science, El Mansoura University, Damietta 34517, Egypt*

Received 19 January 1998; received in revised form 6 August 1998; accepted 29 December 1998

Abstract

Coastline movement due to erosion and deposition is a major concern for coastal zone management. Very dynamic coastlines, such as sections of the Nile Delta coast, pose considerable hazards to human use and development, and rapid, replicable techniques are required to update coastline maps of these areas and monitor rates of movement. The synoptic capability of Landsat Thematic Mapper imagery enables monitoring of large sections of coastline at relatively coarse (30 m) spatial resolution. By comparing positions of the Nile Delta coast in 1984, 1987 and 1990/1991, mapped using a region-growing image segmentation technique, areas of rapid change can be identified and targeted for more detailed monitoring in the field, or using higher resolution images. Rates of erosion and deposition can be estimated crudely, and areas where change appears to be accelerating can also be identified. Areas of severe erosion along the Nile Delta coast are found to be confined to the promontories of the present day mouths of the Nile at Rosetta and Damietta. Eroding shorelines are mostly flanked by accreting shorelines, showing that some of the eroded material is redistributed along the coast. The technique outlined here has potential to augment conventional field-based surveying for monitoring shoreline changes over short timescales.

Keywords: coastlines; coastal sedimentation; littoral erosion; remote sensing; geographic information systems; Nile Delta

1. Introduction

Coastline movement due to erosion and deposition is a major concern for coastal zone management. Very dynamic coastlines, such as sections of the Nile Delta coast, pose considerable hazards to human use and development, and rapid, replicable techniques are required to update coastline maps of these areas. The repetitive acquisition and synoptic capabilities of remote sensing systems can be exploited to provide timely spatial data for coastal geographical information systems (GIS), enabling detection and monitoring of coastline movement. Questions remain over the ability of current orbital systems, with relatively coarse spatial resolutions, to detect these changes over appropriate timescales. This paper presents the results of an experiment to see if Landsat Thematic Mapper data, with 30 m pixels, can detect changes in the position of the Nile Delta coast, since the launch of the satellite in 1984.

* Corresponding author. Tel.: +44-118-9318733; Fax: +44-118-9755865; E-mail: k.h.white@reading.ac.uk
[1] Tel.: +20-57-334205; Fax: +20-57-325803.

0169-555X/99/$ - see front matter
PII: S0169-555X(99)00008-2

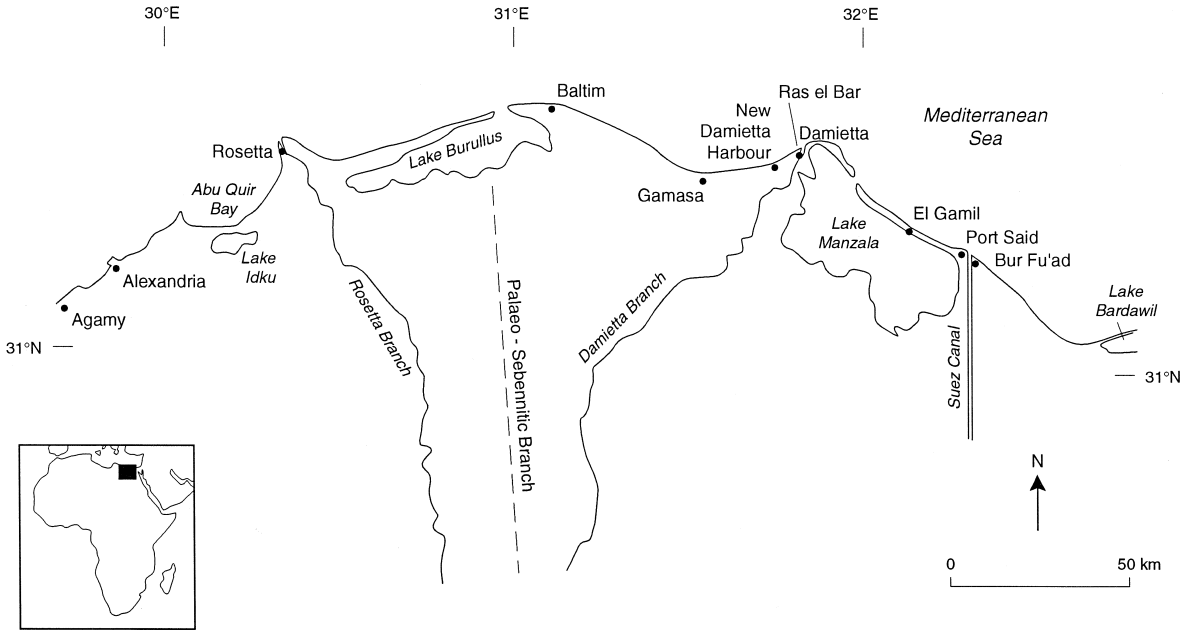

Fig. 1. Location map of places mentioned in the text.

The Nile Delta (Fig. 1) provides an ideal case study to develop remote sensing techniques for coastline monitoring. The dynamic nature of the shoreline is evident from studies of historical maps, which reveal progradation of the promontories by some 3–4 km between 1800 and 1900 (Lotfy and Frihy, 1993). The mouth of the Rosetta branch advanced some 9 km in this period (Frihy and Lotfy, 1994). However, this century has been characterised by net erosion of the Nile Delta coast, the most commonly invoked causal mechanism links coastal erosion to reduction of Nile sediment flux due to the building of six barrages and three dams, prominent among them being the Aswan High Dam, completed in 1964 (Frihy and Khafagy, 1991; Stanley and Wingerath, 1996), although other factors have also been implicated (Lotfy and Frihy, 1993; Stanley, 1996). The shoreline changes impact greatly on human activities; coastal roads, settlements, recreational resorts and valuable agricultural land have been lost as some beaches erode while others accrete (Frihy and Lotfy, 1994). Coastal defence structures, particularly breakwaters, are being deployed along the coastline, with mixed success (Fanos et al., 1995). It has been predicted that the Nile Delta will continue to erode well into the 21st Century, with serious consequences for coastal developments, indicating the need to update maps of the coastline position on a regular basis (Stanley and Warne, 1993).

Directional wave measurements for 1985 to 1990 at Abu Quir and Ras El Bar (Nafaa, 1995) demonstrated that wave action along the Nile Delta coast is seasonal, with high storm waves approaching from the NW–NNW during the winter. These waves generate eastward-flowing longshore currents and a littoral sediment transport flux in that direction (Fanos, 1986). Swells during the Spring and Summer are predominantly from NNW–WNW, with a small component from the NNE; this can cause either easterly or westerly sand transport, depending on the local shoreline orientation. The transport of sediment is eastward at Abu Quir, Burullus, Ras El Bar and Port Said; and westward at Rosetta (El Din and Mahar, 1997).

2. Methodology

Remote sensing techniques have been employed to monitor shoreline changes along the Nile Delta,

Table 1
Imagery acquired for coastal change detection

Path 176 row 38	Path 177 row 38
03/08/1984	07/06/1984
11/07/1987	18/07/1987
04/08/1991	15/05/1990

using data from aerial (Frihy, 1988) and satellite (Blodget et al., 1991) platforms. Long term monitoring is possible by combining both sources, although studies have focused on areas of rapid change, particularly the Rosetta promontory, without taking into account the pattern across the whole delta (El Raey et al., 1995). The main objective of this study is to determine whether relatively short term (of the order of 3 years) coastline changes can be detected with relatively coarse spatial resolution (30 m nominal pixel size) satellite data. Although data of higher spatial resolution are available, cost of data is a factor which often dictates spatial resolution of imagery used in coastal mapping projects, especially in Developing Countries (Wilson, 1997). An analysis of data costs for this project demonstrated that, to cover the same area using 10 m resolution data from the French SPOT satellite, would be 3.6 times as expensive (El Asmar and White, 1997). Furthermore, Thematic Mapper data archives go back to 1984, SPOT data archives go back only to 1986, limiting the potential study period by two years. Use of orbital 1 m data, although possible in the near future with missions such as Orbview, Quickbird and Ikonos scheduled for launch in 1998, would not be feasible for studies of landforms the size of the Nile Delta, due to problems of handling the huge amounts of data this would entail (the TM band 7 dataset used here is 1.75×10^2 Mbytes; to cover the same area at 1 m resolution would require 1.94×10^5 Mbytes). However, an appropriate methodology would be to use relatively coarse resolution data for large-area reconnaissance surveys to identify the most rapidly changing sections of coast, and then to target these areas for analysis with 1 m data, to determine rates of coastline change to higher precision.

Landsat Thematic Mapper data were acquired covering the Nile Delta coastline from Alexandria to northern Sinai (paths 176/177, row 38-Worldwide Reference System) for three dates (Table 1). Two full Thematic Mapper scenes are required to cover the Nile Delta coastline, Path 177 row 38 covers the western half and Path 176 row 38 covers the eastern half, providing a survey of coastline approximately 350 km from west to east. The most recent images of the two multitemporal sets of scenes were registered to geographical coordinates. This was achieved by calculating a second order polynomial to transform the line and column locations of pixels selected from across the images (known as ground control points or G.C.P.s), to their latitude and longitude locations, derived from map and G.P.S. data. The root mean square (R.M.S.) error is also calculated for each G.C.P., to provide a measure of the residuals associated with the transformation (Table 2); the lower the R.M.S. error, the better the fit of the transformation to the G.C.P.s. In this project, no single G.C.P. was permitted to have an R.M.S. error greater than 1 pixel (or 0.5 pixel for image-to-image registration, where G.C.P.s can be more accurately located), and the mean R.M.S. error for all the G.C.P.s was not permitted to exceed 0.55 pixel (or 0.4 pixel for image-to-image registration). This transformation is then applied to the entire image, so that each pixel is associated with latitude and longitude coordinates.

Table 2
R.M.S. errors of image-to-image and image-to-map registration

Registration	Number of GCPs	Maximum R.M.S. error on a GCP (pixels)	Mean R.M.S. error for image (pixels)
07/06/1984 to 15/05/1990	107	0.49	0.35
03/08/1984 to 04/08/1991	94	0.49	0.35
11/07/1987 to 04/08/1991	145	0.49	0.38
18/07/1987 to 15/05/1990	97	0.49	0.33
1990/1991 to map	40	0.81	0.52

The main problem encountered was obtaining reliable geographical coordinates for the G.C.P.s; available maps are either too old or too small-scale to locate G.C.P. features (road or rail intersections, bridges, drain junctions, etc.) with sufficient precision. By using a number of different maps, augmented with other points from a G.P.S. receiver collected during fieldwork, a total of 40 G.C.P.s were selected; 7 points from 1:100,000 Egyptian Department of Survey and Mines (sheet 92/48) dated 1939, 14 points from 1:500,000 Tactical Pilotage Chart (sheet H5-A) dated 1991, 2 points from 1:200,000 Wehrgeologische Wasserkarte (sheet H36NW2) dated 1941, 6 points from 1:100,000 British Military Survey I-GSGS (sheet 31.30–31.00) dated 1956, and 11 G.P.S. locations derived in the field. The same datum (WGS 84) was used throughout. In the absence of significant relief, a second order polynomial provides an adequate transformation for registering a full Thematic Mapper scene to geographical coordinates (Bryant et al., 1985; Hardy, 1985; Welch et al., 1985). All other images were then registered to the geocorrected scenes using second order polynomials.

In order to delineate the land/sea boundary, Thematic Mapper band 7 (shortwave infrared) was used. Shorter wavelengths allow some penetration through water, giving a more gradational effect and making exact delineation of the coastline difficult (Wilson, 1997). Problems of high reflectance offshore due to surf in the breaker zone are also ameliorated by using shortwave infrared data (Frouin et al., 1996).

There are several methods for deriving coastline position from remote sensing data; the coastline can be digitised by eye, the image can be classified into land and sea, often by identifying a threshold value for a single spectral band, or an edge detecting filter or segmentation algorithm can be applied to the image. In order to ensure consistency between coastline location for each date, an automated, replicable methodology must be used (Wilson, 1997). Tracing the coastline manually, although easy along relatively simple stretches of coast, is not practical where the coastline becomes very complex, such as the spit feature on the eastern side of the mouth of the Damietta branch. Here, manual replication of coastline mapping is impossible, even for the same operator, due to the highly convoluted nature of the coast, and problems of mixed (land/sea) pixels. Classification or thresholding techniques can be used, but they output data in raster format which requires a further level of processing to generate a vector format suitable for input into a GIS. Edge detection and segmentation approaches can output data in vector format.

Most algorithms for remotely sensed data are based solely on spectral analysis of individual pixels, whereas the human interpreter makes more use of texture, shape and context of regions in the image. Image segmentation and edge detection algorithms, developed for robot vision, follow more closely the process of human image interpretation (Cross et al., 1988), by dividing an image into different regions (Sonka et al., 1993). There are two techniques, the edge detection (disjunctive) approach finds and links high frequency edges around regions by passing spatial convolution filters over the image. The alternative (conjunctive) approach seeks to grow homogeneous regions by merging pixels or sub-regions on the basis of some similarity criterion (Lemoigne and Tilton, 1995). The latter, region-growing, approach (Fig. 2) has been found to be more suitable for most remote sensing applications (Kettig and Landgrebe, 1976) and is adopted here. For segmentation of different land cover types, such as agricultural land use, various measurements of texture (Weszka et al., 1976) are normally necessary (Chen and Pavlidis, 1979), but segmentation of land and sea in shortwave infrared optical images can usually be implemented using a specified grey level difference from the region mean as a homogeneity criterion, by virtue of their distinct spectral reflectance characteristics at these wavelengths. In this project, mean and standard deviation statistics of beach surfaces and sea surfaces were extracted from the georeferenced imagery and used to specify the homogeneity criterion.

Little pre-processing is necessary for automatic segmentation of water (Wilson, 1997). In order to ensure that the same homogeneity criterion could be applied to all images, a cosine correction was applied for differences in sun angle arising from the different times of the year that the images were collected. This only had a minimal effect on DN values, as all images were acquired in the Northern Hemisphere summer months between May and August. A DN difference from region mean of 20 was found to

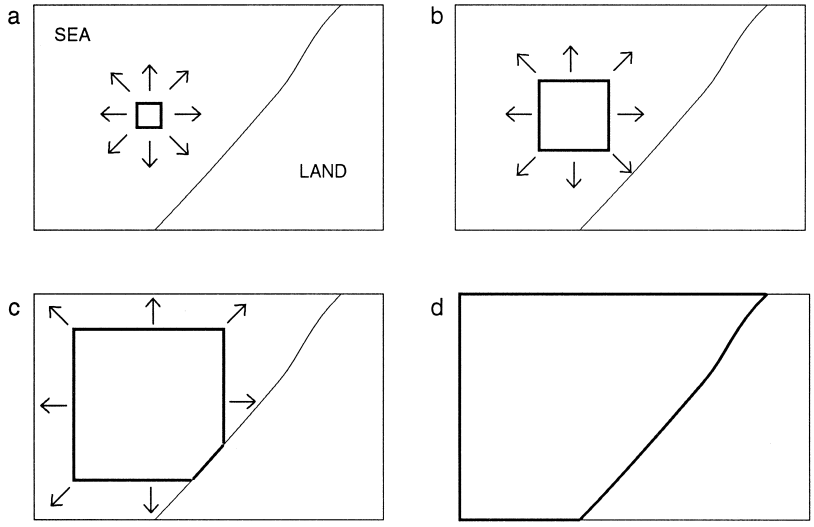

Fig. 2. Schematic diagram showing region growing segmentation. (a) A seed pixel is selected, and surrounding pixels are merged if they satisfy a homogeneity criterion. (b) the region continues to grow by merging surrounding pixels until (c) it encounters pixels which fail to satisfy the homogeneity criterion. (d) The algorithm finishes when the region can grow no further.

account for variability in the sea reflectance in TM band 7, while still ensuring that the coast was always picked up as a region boundary. The region mean was updated with each additional merge. Region growing was initiated at the same point over the sea for each date, in order to avoid differences arising from merging order. Cloud regions over the sea were deleted and interior shorelines of Lakes Burrulus, Manzala, Idko and Bardawil, picked up as the region growth extended down canals and drainage channels, were deleted manually to leave only the coastline. This was output as a vector file, enabling rapid updating of cartographic databases, or analyses of coastline changes in a GIS (Janssen and Molenaar, 1995). The resulting vectors are located at intercell, rather than on-cell boundaries (Fleck, 1992), forming a crack-edge representation of the coastline of the Nile Delta at the time of image acquisition.

When attempting to define the geographic accuracy of this coastline map, it is important to distinguish between precision and accuracy.

2.1. Precision

The instantaneous field of view (Forshaw et al., 1983) of Thematic Mapper data is 30 m, but this is resampled to 28.5 m in the standard NASA format used here (Townshend et al., 1988), although it should be noted that this does not improve the actual spatial resolution of the data (Townshend, 1980). Thus the position of the crack edge can only be defined to 30 m precision. To avoid problems of unjustified precision of data, all measurements used herein are quantised to 30 m, representing the instantaneous field of view of the instrument.

2.2. Accuracy

When determining the accuracy of the spatial location of the coastline, two major aspects must be considered; the effective resolution of the Thematic Mapper system, and the R.M.S. error of the registration.

(a) The effective resolution element (Townshend et al., 1988) is larger than the instantaneous field of view, post-launch analysis indicates an effective instantaneous field of view (one half the reciprocal of the spatial frequency at which the modulation transfer function is 0.5) of between 40 and 50 m for the data products used here (Schowengerdt et al., 1985). Using an analytical model of the Thematic Mapper system, Wilson (1988) arrived at an effective resolution element of 52 m, whereas using land/water interfaces in real Thematic Mapper images, a value of 75 m was obtained. This gives some indication of

Table 3
Additional control points used for checking accuracy of image-to-map registration

Point	Map longitude	Map latitude	Map scale	Displacement (m)	Bearing
El Mahmudia	30°31′35″	30°10′57″	1:250,000	30	200°
Khataba	30°25′56″	31°05′2″	1:250,000	0	102°
El Mex	29°50′49″	31°09′09″	1:100,000	0	111°
Sidi Gâbir	29°55′54″	31°13′00″	1:100,000	0	007°
El Wastani	30°03′25″	31°13′44″	1:100,000	30	305°
Ez Abu Zeid	30°03′14″	31°12′27″	1:100,000	30	090°
Ez Deif	30°03′32″	31°11′31″	1:100,000	30	008°
El Karyûn	30°11′27″	31°07′59″	1:100,000	0	003°
Pumpstation	31°04′37″	31°33′52″	1:100,000	30	357°
Bahr Tira	31°09′01″	31°30′59″	1:100,000	0	225°
Sherbin	31°31′34″	31°10′00″	1:250,000	30	163°
Abu el Nom	31°37′16″	31°17′03″	1:250,000	30	252°
Kom Ebn Salen	32°04′53″	31°10′49″	1:250,000	30	149°
Demellash 2	31°24′43″	31°15′33″	1:250,000	30	283°
Mohit 1	31°34′16″	31°21′53″	1:250,000	0	226°

the accuracy with which the coastline can be demarcated by the Thematic Mapper system.

(b) The R.M.S. error of resampling of pixel DN associated with geometric correction has also to be taken into account, both image-to-image and image-to-map. The R.M.S. errors were kept extremely low in this project, by use of large numbers of G.C.P.s (Table 2). However, these errors must be considered where coastline locations derived from the imagery are being compared with other geographical data.

R.M.S. error is an indicator of the goodness-of-fit of the transformation to the selected ground control points, thus it is only a crude indicator of positional accuracy throughout the image. To check the accuracy of the image-to-map registration, the coordinates of 15 additional control points were determined from the base maps. These points were sampled evenly across the study area, and were not used in the calculation of the original transformation,. The map coordinates were plotted onto the image, and displacement from the point feature was measured and quantised to the 30 m pixel size, as above. These additional control points are subject to the same sorts of measurement error as the original control points, but the results (Table 3) indicate no errors of more than one pixel and no systematic displacement between the imagery and extant maps.

Diurnal and annual cycles of sea level need to be considered as a potential source of error for location of the shoreline from remotely-sensed images, espe-

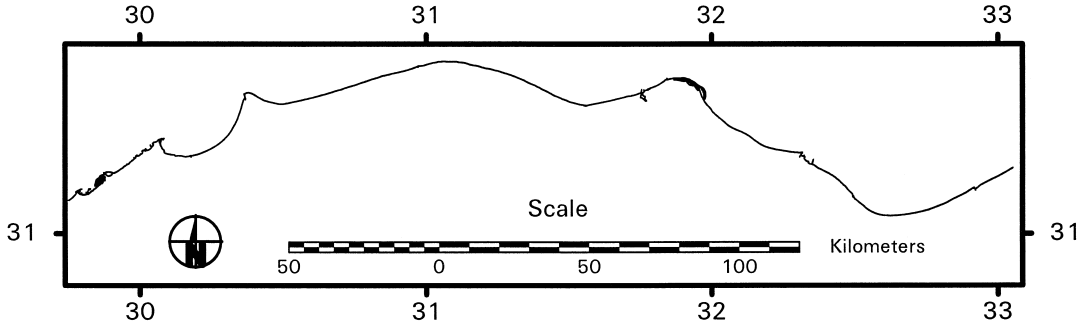

Fig. 3. Vector maps of the Nile Delta coastline produced by region-growing segmentation of Landsat Thematic Mapper data.

cially where the intertidal zone has a very shallow gradient (Mason et al., 1995). The Mediterranean Sea at the Nile Delta is virtually tideless (30–40 cm); detailed monitoring using an automatic tide gauge at Burullus inlet (Fig. 1), some 50 m from the sea, for the 20-year period up to and including the study period 1984–1990/1991, showed a mean tidal range of only 14 cm (El-Fishawi, 1994a). A 60 cm variation in daily mean sea level has been measured at Port Said over the period 1980–1986 (Eid et al.,

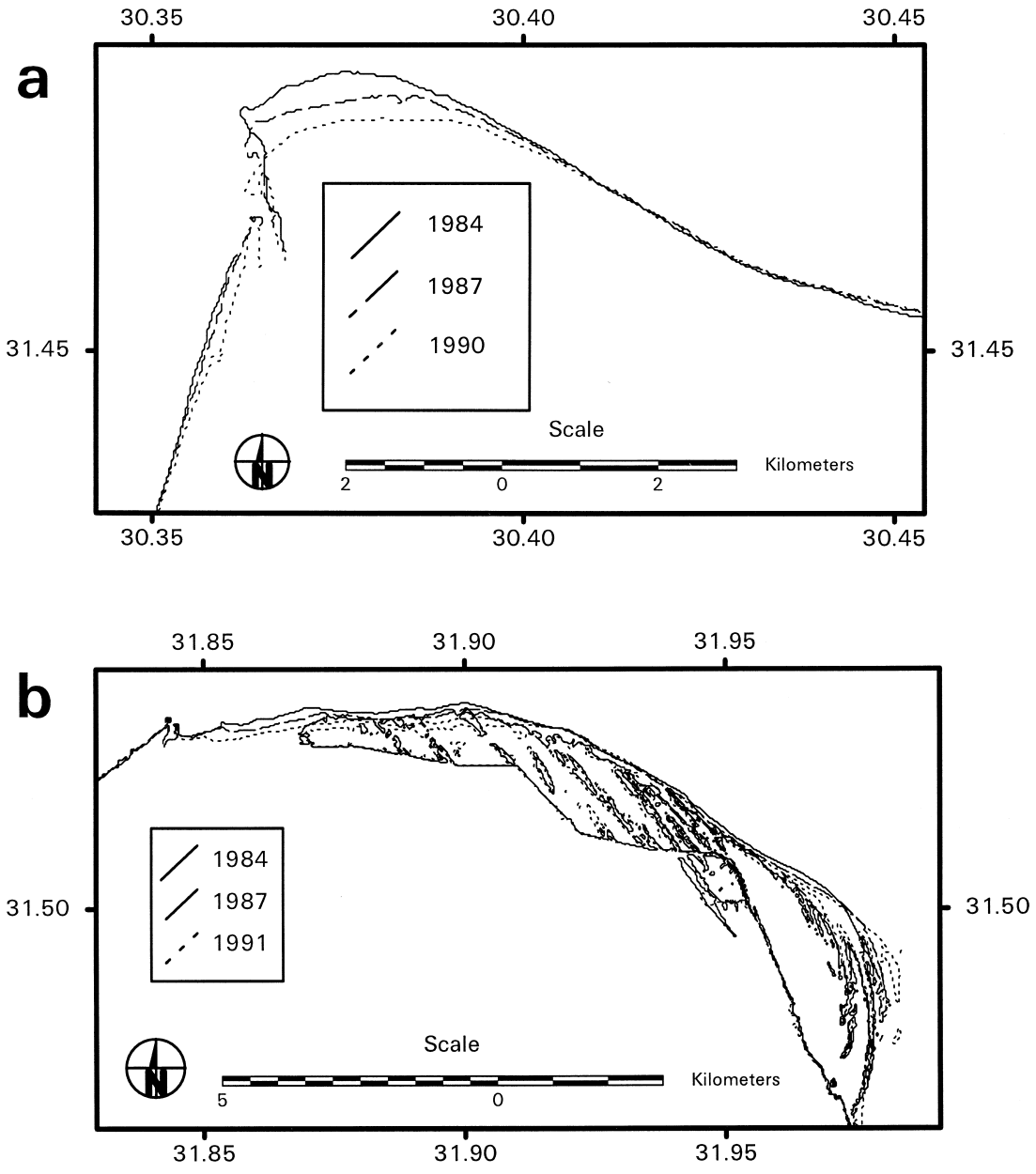

Fig. 4. A section of the vector maps showing rapid erosion of (a) the Rosetta promontory, and (b) the Damietta promontory. Note the complex nature of the coastline in (b), which precludes manual attempts to map the coastline position with any degree of replicability.

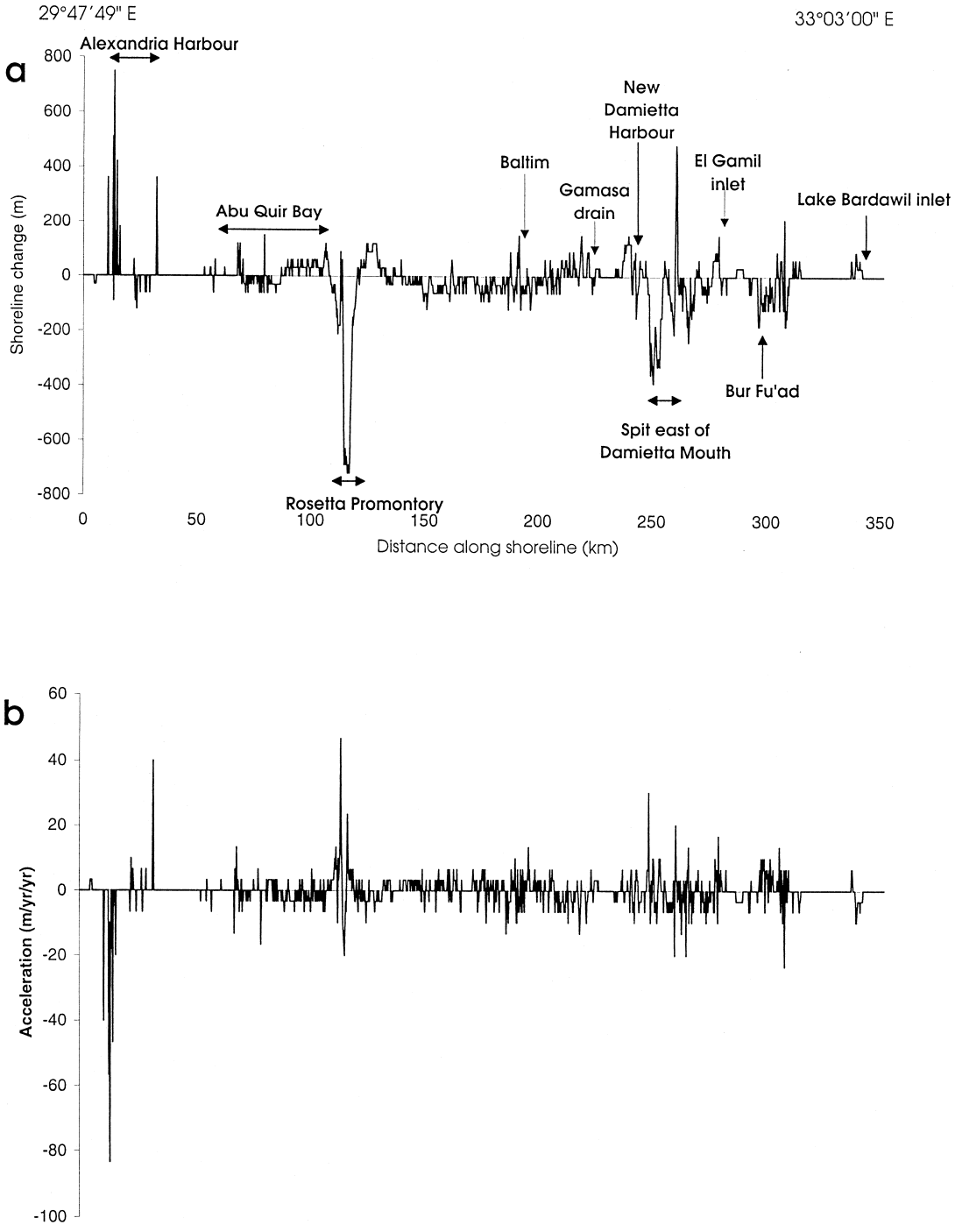

Fig. 5. (a) Shoreline change in the period 1984–1990/1991 (m) sampled at 250 m intervals along coast. Negative values indicate erosion, positive values indicate accretion. (b) Acceleration of rates of shoreline change (m yr^{-2}) comparing the period 1984–1987 to the period 1987–1990/1991. Positive values indicate acceleration of rates of change, negative values indicate deceleration of rates of change.

1997). Detailed surveys of the inter-tidal zone were carried out using a theodolite at eight locations along the Nile Delta coast; it was found that a 60 cm vertical range of mean sea level would equate to a horizontal range of between 4–20 m. During the study period 1984–1990/1991, the mean sea level has been rising 4.9 mm yr^{-1} at the automatic tide gauge at Burullus outlet (El-Fishawi, 1994a), while an increase of 2.8 mm yr^{-1} was measured at Port Said between 1980–1986. Because of the low levels of variance associated with the effects of tides, differences in daily mean sea level, and long term changes in sea level, these factors are not thought to constitute a significant source of error in this project.

3. Results

The resulting coastline vector maps (Fig. 3) permit identification of areas of rapid change, such as the Rosetta and Damietta promontories (Fig. 4). The results confirm the general impression derived from detailed field surveying that erosion is most significant on the promontories of Rosetta, Damietta and the palaeo-Sebennitic branches of the Nile (Sestini, 1989). The redistribution of some of this sediment to the accreting beaches of the embayments, such as at Abu Quir, is also apparent. Measurements of the rate of change can be easily derived from these vector maps using standard G.I.S. measurement tools. The measurements are taken at 250 m intervals; this was found to be an appropriate resolution to detect detailed patterns of change, while reducing the data to a manageable 1400 multitemporal shore profiles for the entire Nile Delta coast. This level of detail compares well to the 65 multitemporal profiles which have been monitored using conventional field-based surveying (Frihy and Komar, 1993). The results for the Nile Delta for the period 1984–1990/1991 (Fig. 5a) show the complex pattern of change along the entire Nile Delta shoreline. Changes within Alexandria Harbour are mostly due to construction work. The presence of large ships along the harbour side causes errors in the technique, as the segmentation algorithm will place the shoreline on the seaward side of the ships when they are moored. However, the most rapid areas of erosion (at the Rosetta and Damietta mouths of the Nile) are clearly evident, although numerous other areas show less dramatic changes. The area around Baltim (Fig. 6), where erosion is causing extensive damage to buildings, shows a complex pattern of sediment redistribution, generally dominated by erosion, but with accreting sections of shoreline adjacent to eroding sections.

Fig. 6. Field photograph showing severe erosion affecting buildings in Baltim.

The impact of anthropogenic coastal structures is also evident in Fig. 5a, New Damietta Harbour is a good example, with significant accretion against the western harbour wall, and significant erosion adjacent to the eastern harbour wall. A similar pattern is seen at Gamasa Drain (outlet of a drainage canal), El-Gamil inlet and at the Lake Bardawil inlet. This provides evidence of the effect of the projecting harbour walls on interrupting the west to east longshore drift at these locations.

In order to identify which of these changes are likely to be most problematic, changes in the two periods between the three image acquisitions can be calculated separately, and areas of accelerating change in the most recent period can be determined (Fig. 5b). Because only two periods are represented here, and because of the relatively coarse (30 m) quantisation of the data upon which these calculations are based, these results must be treated with caution, but the pattern is consistent with field surveys. Apart from the construction work in Alexandria Harbour, the Rosetta and Damietta mouths are identified as areas of accelerating change. Roy et al. (1994) demonstrate that onshore movement of coastal barriers over substrates which progressively flatten in a landward direction will inevitably lead to an observed acceleration of shoreline recession over time.

4. Discussion

Few published rates of shoreline change exist for the Nile Delta coast. Table 4 presents a summary of the comparisons that can be made. Despite the 30 m quantisation of the data used here, the results show similar results when averaged over 250 m sections of shoreline. El-Fishawi (1994a) found rates of retreat of -3.8 m yr^{-1} and -1.3 m yr^{-1} along the eastern and western beaches of Burullus respectively, over the period 1909–1989. This compares with values of -5.0 m yr^{-1} and -2.1 m yr^{-1} averaged over the same stretch of coastline over the period 1984–1990/1991 found in this study. Frihy and Komar (1993) measured beach profile surveys at 65 positions along the entire Nile Delta coastline between 1971 and 1990, and found that the rate of shoreline retreat has been greatest along the Rosetta promontory (-106.0 m yr^{-1}) and Damietta promontory (-10.4 m yr^{-1}). This compares with rates of -113.8 m yr^{-1} and -15.0 m yr^{-1} found in this study. Frihy and Komar also noted significant erosion rates of -6.5 m yr^{-1} along the central bulge of the delta coast, compared to a rate of -5.1 m yr^{-1} found in this project, averaged along the same stretch of coast.

Table 4
Comparison of field survey and image-derived estimates of rates of shoreline change

Location	Field survey-derived rate m yr^{-1}	Image-derived rate m yr^{-1}
West Burullus	-1.3[a]	-2.1[b]
East Burullus	-3.8[a]	-5.0[b]
Baltim	-6.5[c]	-5.1[b]
Rosetta	-106.0[c]	-113.8[b]
Damietta	-10.4[c]	-15.0[b]

[a] El-Fishawi (1994a) for period 1909–1989.
[b] This study for period 1984–1990/1991.
[c] Frihy and Komar (1993) for period 1971–1990.

Lotfy and Frihy (1993) show that zones of accretion occur adjacent to zones of erosion along the Nile Delta coast, the eroded sand comes from the outer tips of the promontories and is transported eastward (or westward at some localities) and is deposited in embayments between the promontories (Lotfy and Frihy, 1993), with the maximum shoreline advance averaging about 13 m yr^{-1} (Frihy and Komar, 1993). Nine different physiographic (erosion/accretion) units have been recognised on the Nile Delta (Fanos, 1995), similar source/sink couplers have been studied on the north Sinai coast (Frihy and Lotfy, 1994). Considerable variation is seen in littoral drift rates along the Nile Delta coastline. Tracer experiments have indicated an easterly drift of 0.35×10^6 m^{-3} yr^{-1} between Agamy and Abu Quir, 0.50×10^6 m^{-3} yr^{-1} along the Rosetta Promontory, and 1.33×10^6 m^{-3} yr^{-1} on the western coast of Burullus lagoon (El-Fishawi, 1994b). The cross shore volume changes indicate that sediment is moving offshore as well as alongshore as littoral drift (Frihy et al., 1994). This is supported by the results of this project; the data shown in Fig. 5a represent a net loss of land surface of some 479 ha between 1984–1990/1991; interestingly there was a net gain of land of 9.7 ha during the period 1984–

1987, but this was more than offset by a loss of 489 ha in the period 1987–1990/1991. Analysis of annual beach profiles between 1978 and 1990 indicate that, along most of the Nile Delta coast, sediment eroded from the upper part of the beach profile (0–2 m below m.s.l.) is deposited in the deeper part (4–6 m below m.s.l), except along the rapidly eroding promontories at the mouths of Damietta and Rosetta branches of the Nile, where erosion increases with depth (Lotfy and Frihy, 1993). Erosion and accretion on the inner continental shelf shows a different pattern, unrelated to sediment texture, gradient and water depth (Frihy et al., 1991).

The resulting vector maps can be used in a coastline management GIS; a system has been proposed for the Nile Delta (Frihy, 1996), similar to that developed for the Netherlands (van Heuvel and Hillen, 1995). However, the technique is subject to two major limitations. Firstly, it can only be applied to coasts with a very low tidal range; the tidal range should not result in horizontal movement of the coastline by more than 20 m (the greatest value encountered in our field surveys of the Nile Delta coast), unless contemporary tide data are available, along with intertidal elevation data, so that coastline positions can be standardised to the same tidal state. Along coasts with a high tidal range, remote sensing data can be used to improve existing intertidal DEMs using the water-line method of Mason et al. (1995). Secondly, the rate of change that can be monitored is limited by the pixel size of the Thematic Mapper; at least a nominal 30 m movement of the coastline position is necessary for reliable detection. Acquisition of suitable imagery from optical instruments is subject to cloud cover restrictions, which could limit utility in cloudy areas if very frequent coastline surveys are required, although radar data could be used in this case (Mason et al., 1995).

The need to improve position precision requires either use of higher resolution data, which is possible for smaller, rapidly changing sections of the coast, or removal of quantisation uncertainties by locating the shoreline to sub-pixel precision. This can be achieved with moment-based edge operators (Lyvers et al., 1989). The simplest way of locating edges to sub-pixel resolution is to use an approximation to the gradient (Tabatabai and Mitchell, 1984), but more complex approaches are necessary for locating complex edges to sub-pixel accuracy (Ghosal and Mehrotra, 1994). A spectral mixture modelling approach (Settle and Drake, 1993) enables the proportions of the land cover classes within the boundary pixels to be calculated, whereupon vectors representing the coastline can be located using a standard method of graphic interpolation (Blamont and Grégoire, 1995). This approach is being examined as part of ongoing research.

5. Conclusions

The results of this project demonstrate that region-growing segmentation can be applied to 30 m pixel Landsat Thematic Mapper data in order to map changes of dynamic coastal landforms, such as sections of the Nile Delta coast. The technique produces vector files of the coastline which can be analysed using GIS tools to estimate rates of change (and acceleration) over relatively short time periods. The synoptic capability of remote sensing provides a useful reconnaissance tool to target more detailed field surveys to areas of rapid and/or accelerating change. The technique also provides an overview of sediment redistribution along the coastline.

Acknowledgements

This project was funded by The Royal Society, with additional fieldwork funded by the British Council. The authors are grateful to Ehab Mostafa Assah for fieldwork assistance, and the staff of the Damietta Faculty of Science, El Mansoura University, Department of Geography, The University of Reading, UK, and the Department of Geography, University of Canterbury, New Zealand for their support.

References

Blamont, D., Grégoire, C.H., 1995. Données télédéctées et précision de la cartographie des limites intra-pixellaires. Bulletin de Société Française de Photogrammétrie et Télédétection 137, 98–102.

Blodget, H.W., Taylor, P.T., Roark, J.H., 1991. Shoreline changes along the Rosetta–Nile promontory. Monitoring with satellite observations. Marine Geology 99, 67–77.

Bryant, N.A., Zobrist, A.L., Walker, R.E., Gokman, B., 1985. An analysis of Landsat Thematic Mapper P-product internal geometry and conformity to Earth Surface Geometry. Photogrammetric Engineering and Remote Sensing 51, 1435–1447.

Chen, P.C., Pavlidis, T., 1979. Segmentation by texture using a co-occurrence matrix and a split-and-merge algorithm. Computer Graphics and Image Processing 10, 172–182.

Cross, A.M., Mason, D.C., Dury, S.J., 1988. Segmentation of remotely-sensed images by a split-and-merge process. International Journal of Remote Sensing 9, 1329–1345.

Eid, F.M., El-Din, S.H.S., El Din, K.A.A., 1997. Sea level variation along the Suex Canal. Estuarine, Coastal and Shelf Sciences 44, 613–619.

El Asmar, H., White, K., 1997. Updating of maps of dynamic coastal landforms by segmentation of Thematic Mapper imagery, examples from the Nile Delta, Egypt. In: Griffiths, G.H., Pearson, D. (Eds.), RSS97- Observations and Interactions. Proceedings of 23rd Annual Conference of the Remote Sensing Society, The University of Reading, 2–4 September 1997, pp. 515–520.

El Din, S.H.S., Mahar, 1997. Evaluation of sediment transport along the Nile Delta coast, Egypt. Journal of Coastal Research 13, 23–26.

El-Fishawi, N.M., 1994a. Relative changes in sea level from tide gauge records at Burullus, central part of the Nile Delta Coast. INQUA MBSS Newsletter 16, 53–61.

El-Fishawi, N.M., 1994b. Characteristics of littoral drift along the Nile Delta coast: I. Alexandria–Burullus. INQUA MBSS Newsletter 16, 38–44.

El Raey, M., Nasr, M., El Hattab, M.M., Frihy, O.E., 1995. Change detection of Rosetta Promontory over the last 40 years. International Journal of Remote Sensing 16, 825–834.

Fanos, A.M., 1986. Statistical analysis of longshore current data along the Nile Delta coast. Water Science Journal, Cairo 1, 45–55.

Fanos, A.M., 1995. The impact of human activities on the erosion and accretion of the Nile Delta coast. Journal of Coastal Research 11, 821–833.

Fanos, A.M., Khafagy, A.A., Dean, R.G., 1995. Protective works on the Nile Delta Coast. Journal of Coastal Research 11, 516–528.

Fleck, M.M., 1992. Some defects in finite-difference edge finders. IEEE Transactions on Pattern Analysis and Machine Intelligence 14, 337–345.

Forshaw, M.R.B., Haskell, A., Miller, P.F., Stanley, D.J., Townshend, J.R.G., 1983. Spatial Resolution of remotely sensed imagery, a review paper. International Journal of Remote Sensing 4, 497–520.

Frihy, O.E., 1988. Nile Delta shoreline changes. Aerial photographic study of a 28 year period. Journal of Coastal Research 4, 597–606.

Frihy, O.E., 1996. Some proposals for coastal management of the Nile Delta coast. Ocean and Coastal Management 30, 43–59.

Frihy, O.E., Khafagy, A.A., 1991. Climate and human induced changes in relation to shoreline migration trends at the Nile Delta promontories, Egypt. Catena 18, 197–211.

Frihy, O.E., Komar, P.D., 1993. Long-term shoreline changes and the concentration of heavy minerals in beach sands of the Nile Delta, Egypt. Marine Geology 115, 253–261.

Frihy, O.E., Lotfy, M.F., 1994. Mineralogy and textures of beach sands in relation to erosion and accretion along the Rosetta Promontory of the Nile Delta, Egypt. Journal of Coastal Research 10, 588–599.

Frihy, O.E., Nasr, S.M., Ahmed, M.H., El Raey, M., 1991. Temporal shoreline and bottom changes of the inner continental shelf off the Nile Delta, Egypt. Journal of Coastal Research 7, 465–475.

Frihy, O.E., Moussa, A.A., Stanley, D.J., 1994. Abu-Quir Bay, a sediment sink off the northwestern Nile Delta. Marine Geology 121, 199–211.

Frouin, R., Schwindling, M., Deschamps, P.Y., 1996. Spectral reflectance of sea foam in the visible and near-infrared. In situ measurements and remote sensing implications. Journal of Geophysical Research 101, 14361–14371.

Ghosal, S., Mehrotra, R., 1994. Detection of composite edges. IEEE Transactions on Image Processing 3, 14–25.

Hardy, J.R., 1985. Geometric quality of a Thematic Mapper image of the United Kingdom. In: Mansel, P. (Ed.), Proceedings of Fall 1985 ACSM/ASPRS Convention: Racing into Tomorrow. LIDQuA Final Symposium, pp. 937–948.

Janssen, L.L.F., Molenaar, M., 1995. Terrain objects, their dynamics and their monitoring by the integration of GIS and remote sensing. IEEE Transactions on Geoscience and Remote Sensing 33, 749–758.

Kettig, R.L., Landgrebe, D.A., 1976. Classification of multispectral image data by extraction and classification of homogeneous objects. IEEE Transactions on Geoscience Electronics 14, 19–26.

Lemoigne, J., Tilton, J.C., 1995. Refining image segmentation by integration of edge and region data. IEEE Transactions on Geoscience and Remote Sensing 33, 605–615.

Lotfy, M.F., Frihy, O.E., 1993. Sediment balance in the nearshore zone of the Nile Delta coast, Egypt. Journal of Coastal Research 9, 654–662.

Lyvers, E.P., Mitchell, O.R., Akey, M.L., Reeves, A.P., 1989. Sub-pixel measurements using a moment-based edge operator. IEEE Transactions on Pattern Analysis and Machine Intelligence 11, 1293–1309.

Mason, D.C., Davenport, I., Flather, R.A., McCartney, B., Robinson, G.R., 1995. Construction of an inter-tidal digital elevation model by the water-line method. Geophysical Research Letters 22, 3187–3190.

Nafaa, M.G., 1995. Wave climate along the Nile Delta coast. Journal of Coastal Research 11, 219–229.

Roy, P.S., Cowell, P.J., Ferland, M.A., Thom, B.G., 1994. Wave-dominated coasts. In: Carter, R.W.G., Woodroffe, C.D. (Eds.), Coastal Evolution. Cambridge University Press, Cambridge, pp. 121–186.

Schowengerdt, R.A., Archwamety, C., Wrigley, R.C., 1985. Landsat Thematic Mapper image-derived MTF. Photogrammetric Engineering and Remote Sensing 51, 1395–1406.

Sestini, G., 1989. Nile Delta, a review of depositional environments and geological history. In: Whateley, M.K.G., Picker-

ing, K.T. (Eds.), Deltas, Sites and Traps for Fossil Fuels. Geological Society Special Publication 41, pp. 99–127.

Settle, J.J., Drake, N.A., 1993. Linear mixing and the estimation of ground cover proportions. International Journal of Remote Sensing 14, 1159–1177.

Sonka, M., Hlavac, V., Boyle, R., 1993. Image Processing, Analysis and Machine Vision. Chapman & Hall, London, 555 pp.

Stanley, D.J., 1996. Nile Delta, extreme case of sediment entrapment on a delta plain and consequent local land loss. Marine Geology 129, 189–195.

Stanley, D.J., Warne, A.G., 1993. Nile Delta, recent geological evolution and human impact. Science 260, 628–634.

Stanley, D.J., Wingerath, J.G., 1996. Nile sediment dispersal altered by the Aswan High Dam, the kaolinite trace. Marine Geology 133, 1–9.

Tabatabai, A.J., Mitchell, O.R., 1984. Edge location to subpixel values in digital imagery. IEEE Transactions on Pattern Analysis and Machine Intelligence 6, 118–204.

Townshend, J.R.G., 1980. The spatial resolving power of Earth resources satellites. NASA Technical Memorandum 82020, Goddard Space Flight Center, Greenbelt, Maryland, 36 pp.

Townshend, J.R.G., Cushnie, J., Hardy, J.R., Wilson, A., 1988. Thematic Mapper Data; Characteristics and Use. NERC Scientific Services, Swindon, 55 pp.

van Heuvel, T., Hillen, R., 1995. Coastline management with GIS in the Netherlands. EARSeL Advances in Remote Sensing 4, 27–34.

Welch, R., Jordan, T.R., Ehlers, M., 1985. Comparative evaluations of the geodetic accuracy and cartographic potential of Landsat-4 and Landsat-5 Thematic Mapper image data. Photogrammetric Engineering and Remote Sensing 51, 1249–1262.

Weszka, J., Dyer, C.J., Rosenfield, A., 1976. A comparative study of texture measures for terrain classification. IEEE Transactions on Systems, Man and Cybernetics 3, 610–621.

Wilson, A.K., 1988. The effective resolution element of Landsat Thematic Mapper. International Journal of Remote Sensing 9, 1303–1314.

Wilson, P.A., 1997. Rule-based classification of water in Landsat MSS images using the variance filter. Photogrammetric Engineering and Remote Sensing 63, 485–491.